The JAK/STAT3 pathway is a common inducer of astrocyte reactivity in Alzheimer's and Huntington's diseases

L. Ben Haim, K. Ceyzeriat, M.A. Carrillo-de Sauvage, F. Aubry, G. Auregan, M. Guillermier, M. Ruiz, F. Petit, D. Houitte, E. Faivre, et al.

Development/Plasticity/Repair

The JAK/STAT3 Pathway Is a Common Inducer of Astrocyte Reactivity in Alzheimer's and Huntington's Diseases

Lucile Ben Haim,[1,2] Kelly Ceyzériat,[1,2] Maria Angeles Carrillo-de Sauvage,[1,2] Fabien Aubry,[1,2] Gwennaëlle Auregan,[1,2] Martine Guillermier,[1,2] Marta Ruiz,[1,2] Fanny Petit,[1,2] Diane Houitte,[1,2] Emilie Faivre,[1,2] Matthias Vandesquille,[1,2] Romina Aron-Badin,[1,2] Marc Dhenain,[1,2] Nicole Déglon,[1,2] Philippe Hantraye,[1,2] Emmanuel Brouillet,[1,2] Gilles Bonvento,[1,2] and Carole Escartin[1,2]

[1]Commissariat à l'Energie Atomique et aux Energies Alternatives (CEA), Département des Sciences du Vivant (DSV), Institut d'Imagerie Biomédicale (I2BM), Molecular Imaging Research Center (MIRCen), F-92260 Fontenay-aux-Roses, France, and [2]Centre National de la Recherche Scientifique (CNRS), Université Paris-Sud, UMR 9199, Neurodegenerative Diseases Laboratory, F-92260 Fontenay-aux-Roses, France

Astrocyte reactivity is a hallmark of neurodegenerative diseases (ND), but its effects on disease outcomes remain highly debated. Elucidation of the signaling cascades inducing reactivity in astrocytes during ND would help characterize the function of these cells and identify novel molecular targets to modulate disease progression. The Janus kinase/signal transducer and activator of transcription 3 (JAK/STAT3) pathway is associated with reactive astrocytes in models of acute injury, but it is unknown whether this pathway is directly responsible for astrocyte reactivity in progressive pathological conditions such as ND. In this study, we examined whether the JAK/STAT3 pathway promotes astrocyte reactivity in several animal models of ND. The JAK/STAT3 pathway was activated in reactive astrocytes in two transgenic mouse models of Alzheimer's disease and in a mouse and a nonhuman primate lentiviral vector-based model of Huntington's disease (HD). To determine whether this cascade was instrumental for astrocyte reactivity, we used a lentiviral vector that specifically targets astrocytes *in vivo* to overexpress the endogenous inhibitor of the JAK/STAT3 pathway [suppressor of cytokine signaling 3 (SOCS3)]. SOCS3 significantly inhibited this pathway in astrocytes, prevented astrocyte reactivity, and decreased microglial activation in models of both diseases. Inhibition of the JAK/STAT3 pathway within reactive astrocytes also increased the number of huntingtin aggregates, a neuropathological hallmark of HD, but did not influence neuronal death. Our data demonstrate that the JAK/STAT3 pathway is a common mediator of astrocyte reactivity that is highly conserved between disease states, species, and brain regions. This universal signaling cascade represents a potent target to study the role of reactive astrocytes in ND.

Key words: **animal models; lentiviral vector; neurodegenerative diseases; reactive astrocytes; SOCS3; STAT3**

Introduction

In response to multiple pathological conditions, astrocytes undergo molecular, morphological, and functional changes, referred to as astrocyte reactivity (Sofroniew and Vinters, 2010). They become hypertrophic, upregulate intermediate filament proteins, including GFAP and vimentin, and display functional alterations that are still not fully understood. Astrocyte reactivity occurs in both acute and progressive pathological conditions and is a hallmark of multiple neurodegenerative diseases (ND; Sofroniew and Vinters, 2010). Astrocyte reactivity develops in vulnerable regions at the early stages of ND and progresses along with neurological symptoms and cell death. Reactive astrocytes are observed in close proximity to amyloid depositions in both patients with Alzheimer's disease (AD) and mouse models of AD (Probst et al., 1982; Itagaki et al., 1989). They are also found in the striatum and cortex of patients with Huntington's disease (HD) and some mouse models of HD (Vonsattel et al., 1985; Yu et al., 2003; Faideau et al., 2010).

The involvement of reactive astrocytes in disease progression is highly controversial. Although they are generally considered as detrimental for neuronal function, several studies suggest that reactive astrocytes may have beneficial effects and promote neuronal survival (Escartin and Bonvento, 2008; Hamby and Sofroniew, 2010). In any case, elucidation of the precise molecular cascades that lead to astrocyte reactivity may help identify potential therapeutic targets to modulate disease progression.

Received Aug. 21, 2014; revised Dec. 8, 2014; accepted Dec. 31, 2014.

Author contributions: L.B.H. and C.E. designed research; L.B.H., K.C., M.A.C.d.S., F.A., G.A., M.G., M.R., F.P., D.H., R.A.-B., and C.E. performed research; E.F., M.V., M.D., N.D., P.H., E.B., and G.B. contributed unpublished reagents/analytic tools; L.B.H. and C.E. analyzed data; L.B.H. and C.E. wrote the paper.

This work was supported by French National Research Agency Grants 2010-JCJC-1402-1 and 2011-BSV4-021-03 (C.E.), 2011-MALZ-003-02 (G.B.), and 2011-INBS-0011 NeurATRIS (P.H.), the Association France Alzheimer (G.B. and M.D.), CEA, and CNRS. L.B.H. was a recipient of a PhD fellowship from the CEA (Irtelis program). We thank Dr. C. Bjørbæk and Dr. S. E. Shoelson for providing us with the pcDNA3-SOCS3 plasmid. We thank N. Dufour, C. Joséphine, and Dr. A. Bémelmans for viral vector production. We are grateful to P. Gipchtein and Dr. C. Jan for their help with immunostainings and Dr. M. C. Gaillard for technical advice on qRT-PCR analysis. We thank T. Kortulewski and L. Irbah for providing training and technical advice for confocal analysis.

The authors declare no competing financial interests.

Correspondence should be addressed to Carole Escartin, MIRCen 18, route du Panorama, F-92260 Fontenay-aux-Roses, France. E-mail: carole.escartin@cea.fr.

N. Déglon's present address: Laboratory of Cellular and Molecular Neurotherapies, Department of Clinical Neurosciences, Lausanne University Hospital, CH-1015 Lausanne, Switzerland.

DOI:10.1523/JNEUROSCI.3516-14.2015

 0270-6474/15/352817-13$15.00/0

Astrocytes can sense many extracellular signals, such as cytokines, growth factors, nucleotides, endothelins, or ephrins, that activate various intracellular signaling pathways, such as the mitogen-activated protein kinase, the nuclear factor κB (NF-κB), and the Janus kinase/signal transducer and activator of transcription (JAK/STAT) pathways (Kang and Hébert, 2011). Among them, the JAK/STAT3 pathway appears as a central player in the induction of astrocyte reactivity. It is activated by a variety of cytokines and growth factors that signal through the gp130 receptor (Levy and Darnell, 2002). Activation of the JAK/STAT3 pathway has been observed in reactive astrocytes in several conditions of acute injury (Justicia et al., 2000; Okada et al., 2006; Herrmann et al., 2008; O'Callaghan et al., 2014) and in patients and mouse models of amyotrophic lateral sclerosis (ALS; Shibata et al., 2009, 2010). However, it remains to be demonstrated whether the JAK/STAT3 pathway is directly responsible for astrocyte reactivity during progressive pathological conditions such as ND.

In this study, we show that the JAK/STAT3 pathway is activated in reactive astrocytes in several mouse and nonhuman primate models of AD and HD. Overexpression of suppressor of cytokine signaling 3 (SOCS3), the endogenous inhibitor of the JAK/STAT3 pathway in astrocytes *in vivo*, inhibited this pathway and prevented astrocyte reactivity. It also reduced microglial activation and increased the formation of mutant huntingtin (Htt) aggregates but did not affect neuronal death. These results identify the JAK/STAT3 pathway as a universal inducer of astrocyte reactivity, and its modulation affects several pathological features in ND.

Materials and Methods

Transgenic mouse models. Amyloid precursor protein (APP)/Presenilin 1 (PS1) mice [B6.Cg-Tg (APPswe, PSEN1dE9) 85Dbo (http://jaxmice.jax.org/strain/005864.html)] harbor the chimeric mouse/human APP gene with Swedish mutations K594N and M595L (APPswe) and the human PS1 variant lacking exon 9 on a C57BL/6J (http://jaxmice.jax.org/strain/000664.html) background (Jankowsky et al., 2004). APP/PS1dE9 breeding pairs were obtained from The Jackson Laboratory. Triple transgenic AD (3xTg-AD) mice express the mutated human APPswe, PS1M146V, and tauP301L transgenes on a mixed 129Sv (http://jaxmice.jax.org/strain/002448.html) and C57BL/6J background (Oddo et al., 2003). Breeding pairs of 3xTg-AD mice were obtained from the Mutant Mouse Regional Resource Centers. We used 8-month-old APP/PS1dE9 heterozygous females, 12-month-old 3xTg-AD homozygous females, and their respective age-matched wild-type (WT) control mice. Genotyping by PCR was performed at 4–6 weeks of age for APP/PS1dE9 mice. All experimental procedures were approved by a local ethics committee and submitted to the French Ministry of Education and Research (Approval 10-057). They were performed in strict accordance with the recommendations of the European Union (86/609/EEC) for the care and use of laboratory animals.

Lentiviral vectors and injections in mice. We used self-inactivated lentiviral vectors containing the central polypurine tract sequence, the mouse phosphoglycerate kinase I promoter, and the woodchuck postregulatory element sequence. We used two types of vectors to mediate transgene expression in either neurons or astrocytes. To target neurons, lentiviral vectors were pseudotyped with the G-protein of the vesicular stomatitis virus (Naldini et al., 1996). To target astrocytes, lentiviral vectors were pseudotyped with the G-protein of the Mokola lyssaviruses and contained four copies of the target sequence of the neuronal miRNA124 to repress transgene expression in neurons (Colin et al., 2009). Lentiviral vectors are referred to as "lenti-name of the transgene" in the subsequent sections of this manuscript. Neuron-targeted vectors encoded the first 171 N-terminal amino acids of human Htt cDNA with either 18 (lenti-Htt18Q) or 82 (lenti-Htt82Q) polyglutamine repeats (de Almeida et al., 2002). Astrocyte-targeted vectors encoded either the enhanced green fluorescent protein cDNA (lenti-GFP) or the murine SOCS3 cDNA (lenti-SOCS3; Bjørbaek et al., 1998).

The production and titration of these lentiviruses have been described previously (Hottinger et al., 2000). Lentiviral vectors were diluted in 0.1 M PBS with 1% BSA at a final concentration of 100 ng p24/μl. Mice were anesthetized with a mixture of ketamine (150 mg/kg) and xylazine (10 mg/kg). Lidocaine (5 mg/kg) was injected subcutaneously under the scalp 5 min before the beginning of surgery. C57BL/6J and 3xTg-AD mice received bilateral stereotaxic injections of diluted lentiviral vectors in the striatum or the subiculum, respectively, administered by a 10 μl Hamilton syringe via a 34 gauge blunt needle. The stereotaxic coordinates used were as follows: for the striatum, anteroposterior (AP), +1 mm; lateral (L), ±2 mm from bregma; ventral (V), −2.5 mm from the dura; and for the subiculum, AP, −2.92 mm; L, ±1.5 mm; V, −1.5 mm, with ear bars set at 4 mm and a tooth bar set at 0 mm. Mice received a total volume of 2.5 or 3.5 μl per injection site at a rate of 0.25 μl/min. At the end of the injection, the needle was left in place for 5 min before being removed slowly. The skin was sutured, and mice were allowed to recover.

For the lentiviral vector-based HD model (de Almeida et al., 2002), 8-week-old male C57BL/6J mice were injected with lenti-Htt18Q (100 ng of p24) and lenti-GFP (150 ng of p24) in the left striatum and with lenti-Htt82Q (100 ng of p24) and lenti-GFP (150 ng of p24) in the right striatum.

To inhibit the JAK/STAT3 pathway in the HD model, 8-week-old male C57BL/6 mice were injected bilaterally in the striatum with lenti-Htt82Q (150 ng of p24) and coinjected with the control lenti-GFP (200 ng of p24) in the left striatum and with lenti-SOCS3 (150 ng of p24) and lenti-GFP (50 ng of p24) in the right striatum. To inhibit the JAK/STAT3 pathway in the AD model, 7- to 8-month-old 3xTg-AD female mice were injected in the subiculum with either lenti-GFP (250 ng of p24) or lenti-SOCS3 (200 ng of p24) and lenti-GFP (50 ng of p24). Coinjections with lenti-GFP were performed to visualize the infected area and the morphology of infected cells as SOCS3 cannot be detected by immunohistochemistry because of the lack of specific antibodies. Postmortem analysis was performed 6 weeks after injection for HD mice and 4.5 months after injection for 3xTg-AD mice.

Primate model of HD. Three adult male cynomolgus monkeys (*Macaca fascicularis*, 4.2 ± 0.08 kg) were used in this study according to European (European Union Directive 86/609/EEC) and French (French Act Rural Code R 214-87-131) regulations. The animal facility was approved by veterinarian inspectors (Authorization 92-032-02) and complies with Standards for Humane Care and Use of Laboratory Animals of the Office of Laboratory Animal Welfare (A5826-01).

Magnetic resonance imaging (MRI) was performed on each macaque to calculate stereotaxic coordinates for lentiviral injection. MRI was performed on a 7 Tesla scanner (Varian) with the following parameters: TR, 15 ms; TE, 5500 ms; TI, 10 ms; flip angle, 90°; and 0.45 × 0.45 × 1 mm with coronal acquisition on a 256 × 256 × 40 matrix. For lentiviral injections, animals were anesthetized with a mixture of ketamine (10 mg/kg) and xylazine (1 mg/kg) and were kept under intravenous infusion of propofol (1% Rapinovet, 0.05–0.25 $mg \cdot kg^{-1} \cdot min^{-1}$) throughout the procedure with continuous monitoring of cardiac and respiratory frequencies, blood pressure, and temperature. Animals were placed in a custom-made stereotaxic frame, and a KDS injection micropump connected to a Hamilton syringe and a 26 gauge needle were used to perform five bilateral injections of 5 μl of lenti-Htt82Q at a rate of 1 μl/min. The injection sites comprised two deposits in the precommissural caudate [anterior commissure (AC) +5, AC +3)] and three deposits in the commissural and postcommissural (AC −2, AC −5) putamen. Postmortem analysis was performed 16–18 months later.

Immunofluorescence. For histological processing, animals were killed with an overdose of sodium pentobarbital. Animals were either perfused transcardially with 4% paraformaldehyde (PFA) or their brains were postfixed for 24 h in 4% PFA. Brains were cryoprotected by incubation in a 30% sucrose solution. Coronal brain sections (mice, 30 μm; monkey, 40 μm) were cut on a freezing microtome, collected serially, and stored at −20°C until additional analysis. Antigen retrieval protocols were used for STAT3 and 4G8 staining. For STAT3 immunofluorescence, slices were permeabilized with 100% methanol at −20°C for 20 min. For 4G8 staining, slices were pretreated in 70% formic acid for 5 min. Sections were then blocked with 4.5% normal goat serum (Sigma) and incubated

with primary antibodies directed against the following proteins: 4G8 (1:500, mouse; Signet Covance), EM48 (1:200, mouse; Millipore Bioscience Research Reagents), GFAP–Cy3 (1:1000, mouse; Invitrogen), IBA1 (1:1000, rabbit; Wako), S100β (1:500, mouse; Invitrogen), STAT3 (STAT3α, 1:200, rabbit; Cell Signaling Technology), and vimentin (1:1000, chicken; Abcam). Anti-STAT3 antibody was diluted in Signal Boost antibody diluent (Cell Signaling Technology). Brain sections were incubated for 36 h with STAT3 antibody and overnight at 4°C for all other antibodies. After rinsing, brain slices were incubated for 1–2 h at room temperature with fluorescent secondary Alexa Fluor-conjugated antibodies (Invitrogen). Slices were stained with DAPI (1:2000; Sigma), mounted with FluorSave reagent (Calbiochem), and analyzed by either epifluorescence (DM6000; Leica) or confocal microscopy (LSM 510 by Zeiss; and TCS SPE or SP8 by Leica).

Immunohistochemistry. Brain slices were pretreated in 0.3% H_2O_2, blocked in 4.5% NGS (Sigma), and incubated overnight at 4°C with primary antibodies directed against DARPP32 (1:1000, rabbit; Santa Cruz Biotechnology) or EM48 (1:200). After rinsing, brain slices were incubated with biotinylated secondary antibodies (Vector Laboratories) for 1 h at room temperature. Finally, they were incubated with the Vectastain Elite ABC Kit (Vector Laboratories) and revealed with the DAB kit (Vector Laboratories).

Cytochrome c oxidase histochemistry. Brain slices were incubated in 0.1 M PB, 4% sucrose, 0.05% DAB (Sigma), and 0.03% cytochrome *c* (Sigma) for 6 h at room temperature.

qRT-PCR. Mice were killed with an overdose of sodium pentobarbital. Mouse brains were rapidly collected and sliced into 1-mm-thick coronal sections with a brain matrix. The GFP-positive (GFP^+) area on each slice was dissected with 1-mm-diameter punches (Ted Pella) under a fluorescence macroscope (MacroFluo; Leica). Punches were stored in RNA Later (Sigma) until additional processing. Total RNA was isolated from striatal punches with TRIzol (Invitrogen), and cDNA was synthesized from 0.2 μg of RNA with the VILO kit (Invitrogen) and diluted at 0.3 ng/μl. The Platinum SYBR Green qPCR SuperMix UDG (Invitrogen) was used to perform qRT-PCR. Three housekeeping genes were tested, and the peptidylprolyl isomerase A (*cyclophilin A*) gene was selected as the best normalizing gene, because it showed the minimal, nonsignificant, variation between groups. The abundance of each transcript of interest was then normalized to the abundance of *cyclophilin A* with the ΔCt method. The efficiency of qRT-PCR were between 85 and 110% for each set of primers. Distilled water and RT-negative reactions were used as negative controls. The sequences of oligonucleotides used for qRT-PCR are as follows: *aif1* (*iba1*), forward, CCAGCCTAAGACAACCAGCGTC and reverse, GCTGTATTTGGGATCATCGAGGAA; *ccl2*, forward, ACCAGCACCAGCCAACTCT and reverse, AGGCCCAGAAGCATGACA; *cyclophilin A*, forward, ATGGCAAATGCTGGACCAAA and reverse, GCCTTCTTTCACCTTCCCAAA; *gfap*, forward, ACGACTATCGCCGCCAACT and reverse, GCCGCTCTAGGGACTCGTTC; *itgam* (*CD11b*), forward, GGGAGAATGCTGCGAAGA and reverse, GCTGGCTTAGATGCGATGG; *socs3*, forward, CGAGAAGATTCCGCTGGTACTGA and reverse, TGATCCAGGAACTCCCGAATG; and *vimentin*, forward, TCGAGGTGGAGCGGGACAAC and reverse, TGCAGGGTGCTTTCGGCTTC.

Western blotting. Mice were killed with an overdose of sodium pentobarbital, and their brains were rapidly collected and sliced into 1-mm-thick coronal sections with a brain matrix. The striatum or the dorsal hippocampus were dissected out. Samples were then homogenized with a glass homogenizer in 50 mM Tris-HCl, pH 7.4, 100 mM NaCl, and 1% SDS, with protease (Roche) and phosphatase (Sigma) inhibitor cocktails. Protein concentration was determined by the BCA method. Protein samples were diluted in NuPAGE LDS sample buffer with NuPAGE Sample Reducing agent (Life Technologies), boiled for 5 min, loaded on a 4–12% Bis-Tris gel, submitted to SDS-PAGE, and transferred to a nitrocellulose membrane, with an iBlot transfer device (Life Technologies). Membranes were blotted overnight at 4°C with antibodies against GAPDH (1:4000, mouse; Abcam) or IκBα (1:500, mouse; Cell Signaling Technology) diluted in Tris-buffered saline with 0.1% Tween 20 and 5% BSA. After rinsing, secondary antibodies coupled to horseradish peroxidase were incubated with the membrane for 1 h (for IκBα, 1:500, Cell Signaling Technology; and for GAPDH, 1:5000, Vector Laboratories). Antibody binding was detected by a Fusion FX7 camera system (Thermo Fisher Scientific) after incubation with the enhanced chemiluminescence Clarity substrate (Bio-Rad). Band intensity for IκBα were measured with NIH Image J (http://imagej.nih.gov/ij/) and normalized to GAPDH. Positive controls for NF-κB pathway activation were included. They were prepared from HeLa cells treated with TNFα (Cell Signaling Technology).

Quantification of immunostainings. Immunofluorescent staining was quantified from stacked confocal images (18 steps; Z-step, 1 μm, maximum intensity stack) acquired with the 40× objective on three slices per mouse and three fields on each slice. The $GFAP^+$ area was measured on each 40× Z-stack image with the threshold function of NIH Image J. $GFAP^+$ and $IBA1^+$ areas were divided by the area of the image and expressed as a percentage. The average number of $GFAP^+$ cells expressing STAT3 in the nucleus ($nSTAT3^+/GFAP^+$ cells) was quantified on these images. In lenti-GFP-injected mice, we also quantified the average number of GFP^+ infected astrocytes coexpressing STAT3 ($GFP^+/STAT3^+$ cells), GFAP ($GFP^+/GFAP^+$ cells), or S100β ($GFP^+/S100\beta^+$ cells). Finally, astrocyte soma was manually segmented, and the corresponding mean gray value for STAT3 staining was measured with NIH Image J. We then determined the number of cells with a mean gray value for STAT3 over a fixed threshold for each experiment. These cells were considered as cells expressing high levels of STAT3. Unfortunately, the presence of autofluorescent puncta in the subiculum made it impossible to quantify reliably the intensity of STAT3 staining in 3xTg-AD mice and WT controls. Microscope settings and NIH Image J thresholds were identical for all images and mice, within each experiment. Immunohistochemical stainings were quantified on bright-field images, acquired with the 2.5× (COX and DARPP32 stainings) or 10× (EM48 staining) objectives, on five to eight serial sections per mice. The lesion was detected by a loss of DARPP32 and COX staining and was manually segmented with NIH Image J on each slice. The lesion volume was calculated with the Cavalieri method (Damiano et al., 2013). $EM48^+$ aggregates were automatically detected on each image with the threshold function of the Morphostrider analysis software (Explora Nova), as described previously (Francelle et al., 2014). From these measurements, the average size and the total number of aggregates were calculated.

Statistical analysis. Results are expressed as mean ± SEM. Statistical analysis was performed with Statview software. We used Student's *t* test to compare two experimental groups and a Student's paired *t* test for left–right comparisons. The fraction of cells expressing high levels of STAT3 was normalized by the arcsine transformation, before applying a Student's *t* test. The results of qRT-PCR were analyzed using two-way (Htt length and treatment) ANOVA test and Scheffé *post hoc* test. The significance level was set at $p < 0.05$.

Results

Astrocyte reactivity is observed in vulnerable brain regions in AD and HD mouse models

Reactive astrocytes overexpressing GFAP were found around $4G8^+$ amyloid depositions in both the APP/PS1dE9 and the 3xTg-AD transgenic mouse models of AD, consistent with previous findings (Oddo et al., 2003; Ruan et al., 2009). In particular, astrocytes overexpressed GFAP and displayed hypertrophic processes in the stratum lacunosum moleculare and the dentate gyrus of 8-month-old APP/PS1d9 mice (Figs. 1*A*, 2*A*,*B*). We quantified this phenomenon by counting the number of pixels that were positive for GFAP staining on confocal images of the hippocampus. The $GFAP^+$ area was four times larger in APP/PS1d9 mice than in WT mice ($p = 0.0010$, df = 5, Student's *t* test; Fig. 1*B*). Astrocytes in APP/PS1dE9 mice also strongly expressed vimentin (Fig. 2*B*). The APP/PS1dE9 mouse is a quickly evolving model of AD, with substantial deposits of amyloid at 6 months of age (Jankowsky et al., 2004). Thus, we analyzed astrocyte reactivity in 3xTg-AD mice, a more progressive model of AD. We observed astrocyte reactivity around amyloid depositions primarily

in the subicular region of the hippocampus, in female 3xTg-AD mice at 12 months of age (Figs. 1*C*, 3*A*,*B*). In this region, the GFAP$^+$ area was 13-fold larger in 3xTg-AD mice than in age-matched controls ($p < 0.0001$, df = 6, Student's *t* test; Fig. 1*D*). Furthermore, astrocytes displayed a reactive morphology with enlarged soma and processes and overexpressed vimentin, which was nearly undetectable in WT mice (Fig. 3*B*).

We also characterized astrocyte reactivity in mouse models of HD. We studied two HD transgenic mouse models, N171-82Q mice (Schilling et al., 1999) and Hdh140 knock-in HD mice (Menalled et al., 2003). Although these models recapitulate the typical features of HD, we found that they displayed undetectable or very late astrocyte reactivity in the striatum and cortex, similar to what has been described in other mouse models (Tong et al., 2014). Thus, we focused on a lentiviral-based model of HD that has been used extensively (Ruiz and Déglon, 2012). This model reproduces both neuronal death and strong astrocyte reactivity in the striatum, as observed in HD patients (Faideau et al., 2010). C57BL/6 mice were injected in the left striatum with a lentiviral vector encoding normal Htt with 18 glutamines (lenti-Htt18Q) and in the right striatum with a lentiviral vector encoding mutant Htt (mHtt) with 82 glutamines (lenti-Htt82Q). Mice were studied 6 weeks later. As described previously (Faideau et al., 2010; Francelle et al., 2014), overexpression of Htt82Q in neurons led to the formation of intraneuronal EM48$^+$ aggregates of mHtt (Fig. 1*E*). In the lenti-Htt82Q-injected striatum, astrocytes strongly upregulated both GFAP and vimentin relative to the contralateral striatum injected with lenti-Htt18Q (Figs. 1*E*, 4*A*). The GFAP$^+$ area within the injected area was six times larger in the Htt82Q side than in the Htt18Q side ($p = 0.0098$, df = 5, Student's paired *t* test; Fig. 1*F*).

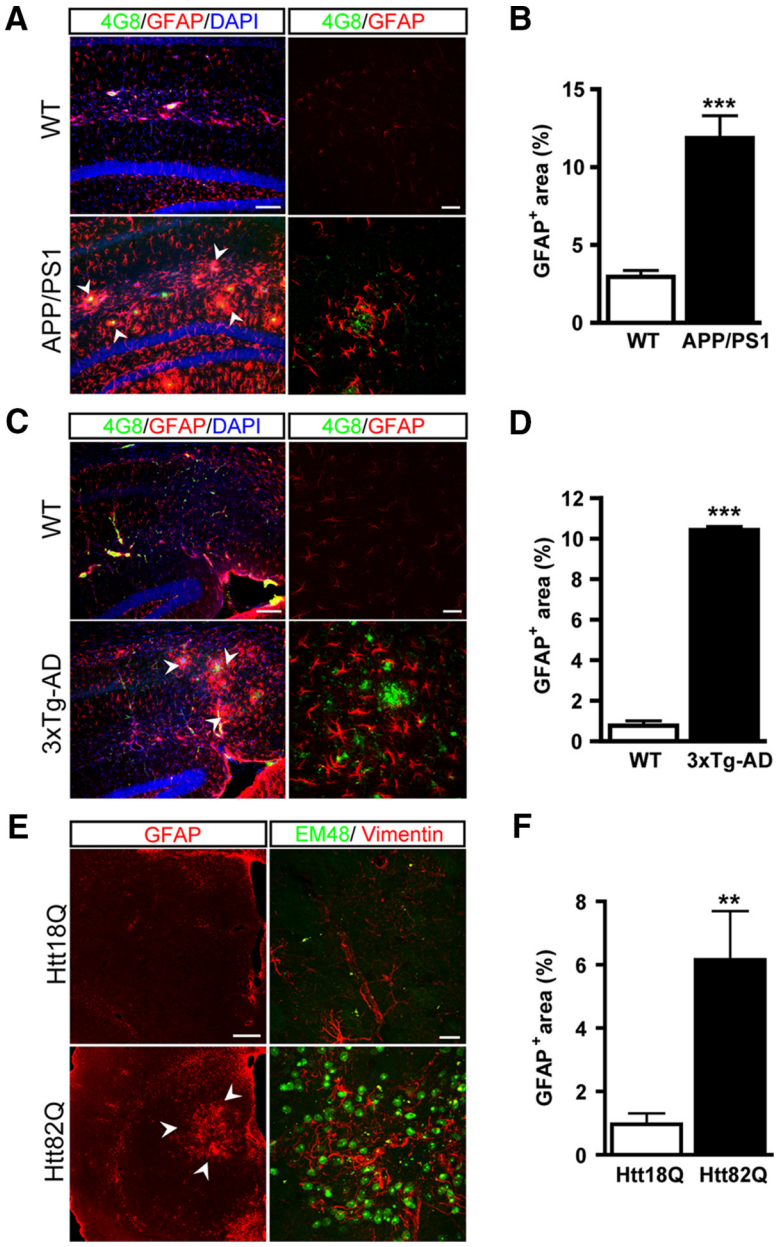

Figure 1. Mouse models of AD and HD display astrocyte reactivity in vulnerable regions of the brain. ***A–C***, Images of brain sections from mouse models of AD showing double staining for amyloid plaques (4G8, green) and astrocytes (GFAP, red). ***A***, GFAP is strongly expressed in hippocampal astrocytes of 8-month-old APP/PS1dE9 mice around amyloid depositions (arrowheads) in the stratum lacunosum moleculare and the dentate gyrus. ***B***, Quantification of the GFAP$^+$ area in the hippocampus of APP/PS1dE9 and WT mice. ***C***, In the subiculum, 3xTg-AD mice display amyloid depositions that are surrounded by GFAP$^+$ reactive astrocytes (arrowheads). ***D***, Quantification of the GFAP$^+$ area in the subiculum of 12-month-old 3xTg-AD mice and age-matched WT mice. ***E***, Mice injected with lenti-Htt82Q in the striatum display EM48$^+$ aggregates of mHtt (green). Expression of the mHtt in striatal neurons leads to astrocyte reactivity (arrowheads) as shown by increased GFAP and vimentin staining (red). ***F***, Quantification of the GFAP$^+$ area in the lenti-Htt82Q-injected striatum relative to the control striatum injected with lenti-Htt18Q. $n = 3–6$ per group. $^{**}p < 0.01$, $^{***}p < 0.001$. Scale bars: ***A*** and ***C***, left, 100 μm; right, 20 μm; ***E***, left, 200 μm; right, 20 μm.

The JAK/STAT3 pathway is activated in reactive astrocytes in AD and HD mouse models

We next evaluated whether astrocyte reactivity observed in these models was associated with activation of the JAK/STAT3 pathway. The phosphorylated form of STAT3 (pSTAT3) was undetectable by immunofluorescence or Western blotting in these progressive models of ND. After activation, pSTAT3 translocates to the nucleus in which it induces the transcription of a set of target genes, including the *Stat3* gene itself (Campbell et al., 2014). Thus, we considered STAT3 nuclear localization and increased immunoreactivity as indexes of JAK/STAT3 pathway activation, as reported previously (Escartin et al., 2006; Tyzack et al., 2014). This also enabled us to identify cell types displaying an active JAK/STAT3 pathway. To validate this surrogate marker of JAK/STAT3 pathway activation, we used ciliary neurotrophic factor (CNTF), a well known activator of this pathway (Bonni et al., 1993) in astrocytes (Escartin et al., 2006). Besides increasing STAT3 phosphorylation, CNTF overexpression in the mouse striatum increased STAT3 levels in the nucleus of reactive astrocytes (data not shown). Interestingly, STAT3 staining was observed predominantly in astrocytes in all models of ND. In

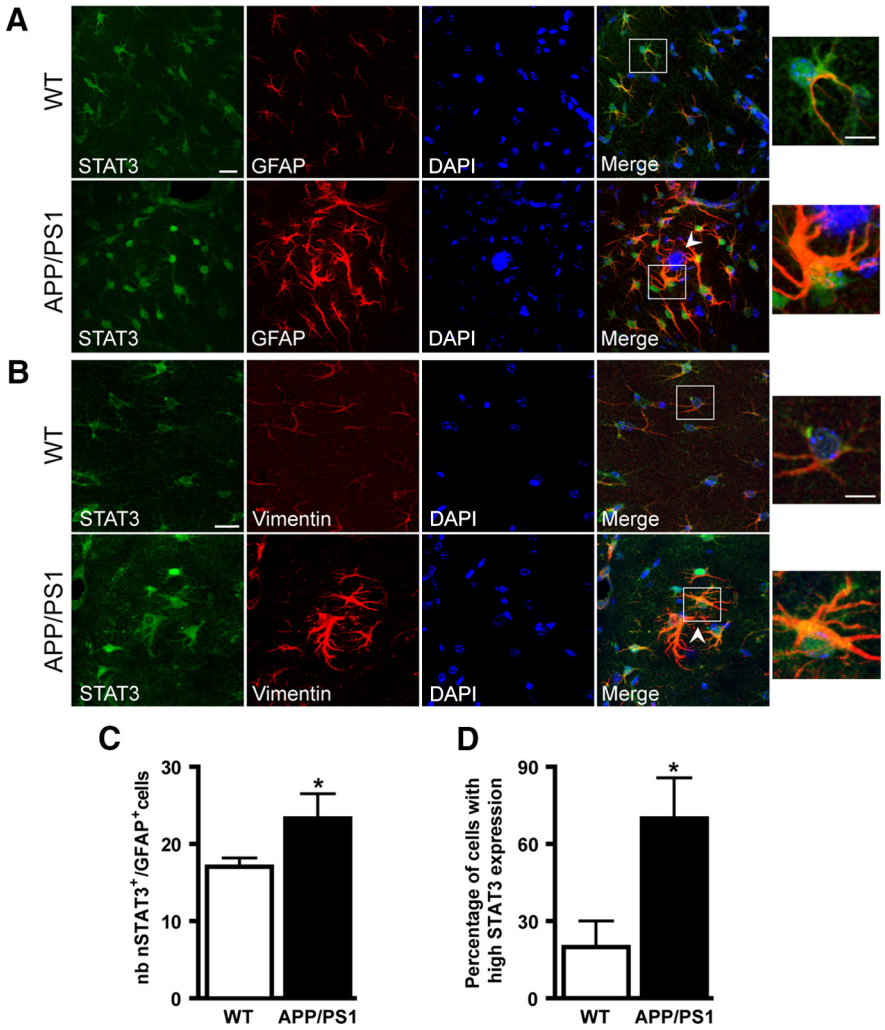

Figure 2. The JAK/STAT3 pathway is activated in reactive astrocytes in APP/PS1dE9 mice. ***A***, ***B***, Images of brain sections from 8-month-old APP/PS1dE9 mice showing double staining for STAT3 (green) and reactive astrocyte markers (***A***, GFAP; ***B***, vimentin). APP/PS1dE9 mice display reactive astrocytes that overexpress GFAP, vimentin, and STAT3 around amyloid plaques (arrowhead) in the hippocampus. STAT3 accumulates in the nucleus of reactive astrocytes (see enlargement). ***C***, The number of GFAP$^+$ astrocytes coexpressing STAT3 in the nucleus (nSTAT3$^+$/GFAP$^+$ cells) is significantly higher in APP/PS1dE9 mice than in WT mice. ***D***, The percentage of cells showing strong staining for STAT3 is higher in APP/PS1dE9 mice than in WT mice. $n = 3$–4 per group. $^*p < 0.05$. Scale bars: 20 μm; enlargements, 5 μm.

8-month-old APP/PS1dE9 mice, there was an accumulation of STAT3 in the nucleus of GFAP$^+$ and vimentin$^+$ reactive astrocytes, whereas in age-matched WT mice, STAT3 was expressed at the basal level throughout the astrocyte cytoplasm (Fig. 2*A*,*B*). The number of GFAP$^+$ astrocytes expressing STAT3 in the nucleus (nSTAT3$^+$/GFAP$^+$ cells) was higher in APP/PS1dE9 mice than in age-matched WT mice ($p = 0.0235$, df = 5, Student's *t* test; Fig. 2*C*). We also measured STAT3 immunoreactivity in astrocyte cell bodies. The percentage of cells with high STAT3 expression was more than threefold higher in APP/PS1dE9 mice than in WT mice, reflecting STAT3 activation in this mouse model of AD ($p = 0.0226$, df = 5, Student's *t* test; Fig. 2*D*).

In the subiculum of 12-month-old female 3xTg-AD mice, there was also a strong increase in STAT3 immunoreactivity in the nucleus of reactive astrocytes overexpressing GFAP and vimentin (Fig. 3*A*,*B*). The number of astrocytes coexpressing GFAP and STAT3 in the nucleus was >10-fold higher in 3xTg-AD mice than in age-matched WT mice ($p < 0.0001$, df = 6, Student's *t* test; Fig. 3*C*).

We then investigated whether the JAK/STAT3 pathway was also activated in the mouse model of HD. STAT3 staining was strongly upregulated in reactive astrocytes found in the lenti-Htt82Q-injected striatum (Fig. 4*A*). Indeed, there were four times more nSTAT3$^+$/GFAP$^+$ astrocytes in the Htt82Q striatum than in the Htt18Q striatum ($p = 0.0004$, df = 5, Student's paired *t* test; Fig. 4*B*). Cells expressing high levels of STAT3 were also more abundant in the Htt82Q striatum than in the Htt18Q striatum ($p = 0.0060$, df = 5, Student's paired *t* test; Fig. 4*C*). We sought to evaluate whether the JAK/STAT3 pathway was also activated in reactive astrocytes in other species. We took advantage of the fact that lentiviral vectors can be used in several animal species, including nonhuman primates. Injection of lenti-Htt82Q in the macaque putamen leads to the formation of mHtt aggregates, neuronal death, and motor symptoms (Palfi et al., 2007). We found that the injection of lenti-Htt82Q into the macaque putamen induced the formation of EM48$^+$ aggregates of mHtt and led to strong astrocyte reactivity (Fig. 5). There was a prominent accumulation of STAT3 in the nucleus of GFAP$^+$ reactive astrocytes. In contrast, at a distance from the injection area, resting astrocytes of the same animal expressed nearly undetectable levels of both GFAP and STAT3 (Fig. 5).

These results suggest that the JAK/STAT3 pathway is a common signaling cascade for astrocyte reactivity in several models of ND, which involve different pathological mechanisms, brain regions, and animal species.

The NF-κB pathway is not activated in 3xTg-AD mice and in the lentiviral-based model of HD

Other pathways, such as NF-κB, have been associated with astrocyte reactivity (Kang and Hébert, 2011). Therefore, we used Western blotting to measure the abundance of IκBα, the master inhibitor of the NF-κB pathway, which is degraded during pathway activation (Hayden and Ghosh, 2008).

We performed this experiment with 3xTg-AD mice and lenti-Htt82Q-injected mice, because astrocyte reactivity was the strongest in these models. In 3xTg-AD mice, the abundance of IκBα normalized to GAPDH was similar to that in WT mice ($p = 0.4037$, df = 8, Student's *t* test; Fig. 6*A*), whereas the positive control of cells treated with the cytokine TNFα displayed the expected decrease in IκBα levels (Fig. 6*A*,*B*). Similarly, the abundance of IκBα normalized to GAPDH was not different between the Htt18Q striatum and the Htt82Q striatum ($p = 0.8062$, df = 5, Student's paired *t* test; Fig. 6*B*).

The JAK/STAT3 pathway is responsible for astrocyte reactivity in AD and HD models

To establish that the JAK/STAT3 pathway was responsible for astrocyte reactivity, we inhibited this pathway by overexpressing

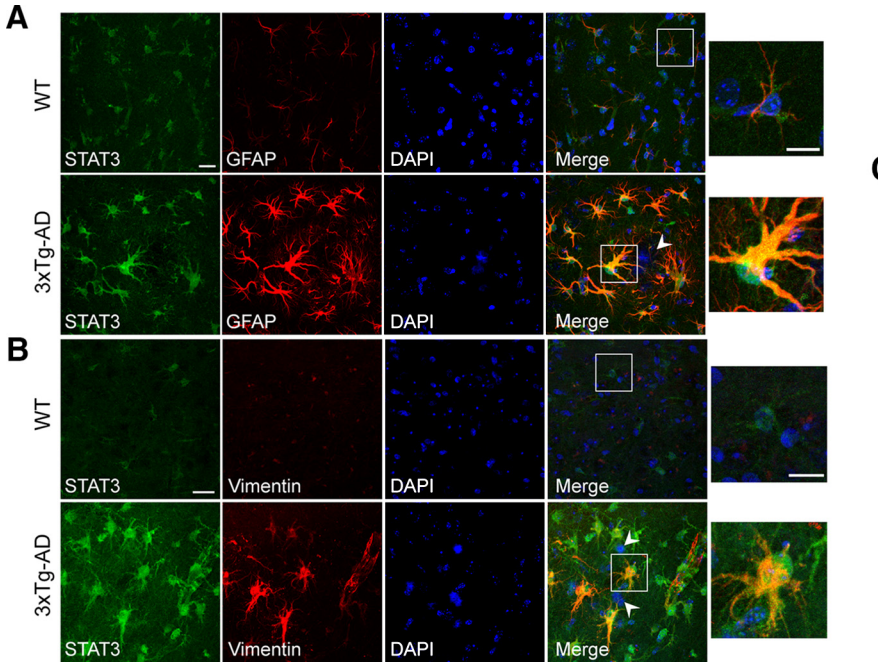

Figure 3. The JAK/STAT3 pathway is activated in reactive astrocytes in 3xTg-AD mice. ***A***, ***B***, Images of brain sections from the subiculum of 12-month-old 3xTg-AD mice. STAT3 (green) accumulates in the nucleus of reactive astrocytes labeled with GFAP (***A***, red) or vimentin (***B***, red), especially around amyloid plaques (arrowheads). ***C***, The number of nSTAT3$^+$/GFAP$^+$ cells is significantly higher in 3xTg-AD mice than in age-matched WT controls. $n = 3$–5 per group. $^{***}p < 0.001$. Scale bars: 20 μm; enlargements, 5 μm.

its endogenous inhibitor SOCS3 through selective lentiviral gene transfer in astrocytes. SOCS3 blocks STAT association with JAK2 (Kershaw et al., 2013) and prevents its phosphorylation, operating a negative feedback on the JAK/STAT3 pathway (Starr et al., 1997).

We used Mokola-pseudotyped lentiviral vectors that selectively target astrocytes (Colin et al., 2009; Figs. 7*F*, 8*G*) We did not detect transgene expression in other brain cell types, such as IBA1$^+$ microglia (Fig. 9*A*), NeuN$^+$ neurons, NG2$^+$ oligodendrocyte progenitors, or MBP$^+$ myelinating oligodendrocytes (data not shown). In addition, we checked that infection of astrocytes with a control lentiviral vector (lenti-GFP) did not lead to their activation in the striatum of WT mice or in the subiculum of 3xTg-AD mice. In both models, GFAP expression was similar between lenti-GFP controls and non-injected mice (data not shown).

We first tested whether SOCS3 overexpression in astrocytes was able to inhibit the JAK/STAT3 pathway. We used CNTF to strongly induce STAT3 phosphorylation, and we found that coinjection with lenti-SOCS3 significantly reduced pSTAT3 levels by Western blot (data not shown). We detected SOCS3 overexpression by qRT-PCR after lenti-SOCS3 injection (100-fold increase; Fig. 8*I*), but we were not able to show SOCS3 expression by immunohistochemistry because of the lack of specific antibodies. Therefore, for each experiment, we coinjected lenti-GFP with lenti-SOCS3 to visualize infected cells and their morphology. Indeed, we found that injection of two lentiviral vectors leads to a large majority of infected astrocytes coexpressing the two transgenes (88.7 ± 2%). Control mice were injected with lenti-GFP alone, at the same total virus load.

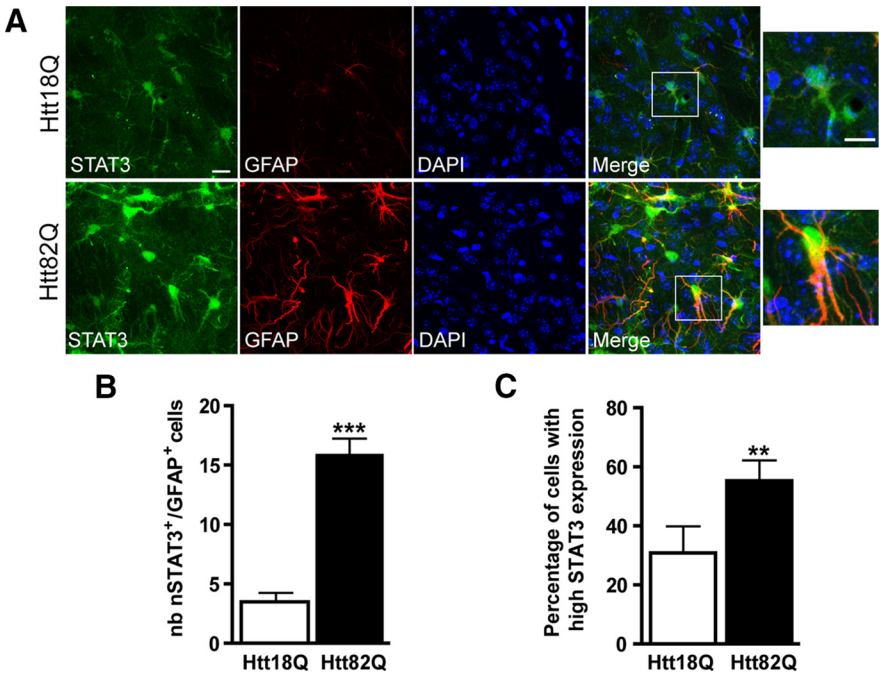

Figure 4. The JAK/STAT3 pathway is activated in reactive astrocytes in the mouse model of HD. ***A***, Images of brain sections showing double staining for GFAP (red) and STAT3 (green) on mouse brain sections, 6 weeks after the infection of striatal neurons with lenti-Htt18Q or lenti-Htt82Q. Astrocytes in the Htt82Q striatum are hypertrophic and express higher levels of STAT3 in their nucleus relative to resting astrocytes in the Htt18Q striatum. ***B***, ***C***, The number of nSTAT3$^+$/GFAP$^+$ cells (***B***) and the percentage of cells displaying strong staining for STAT3 (***C***) are significantly higher in the Htt82Q striatum than in the Htt18Q striatum. $n = 6$. $^{**}p < 0.01$, $^{***}p < 0.001$. Scale bars: 20 μm; enlargements, 5 μm.

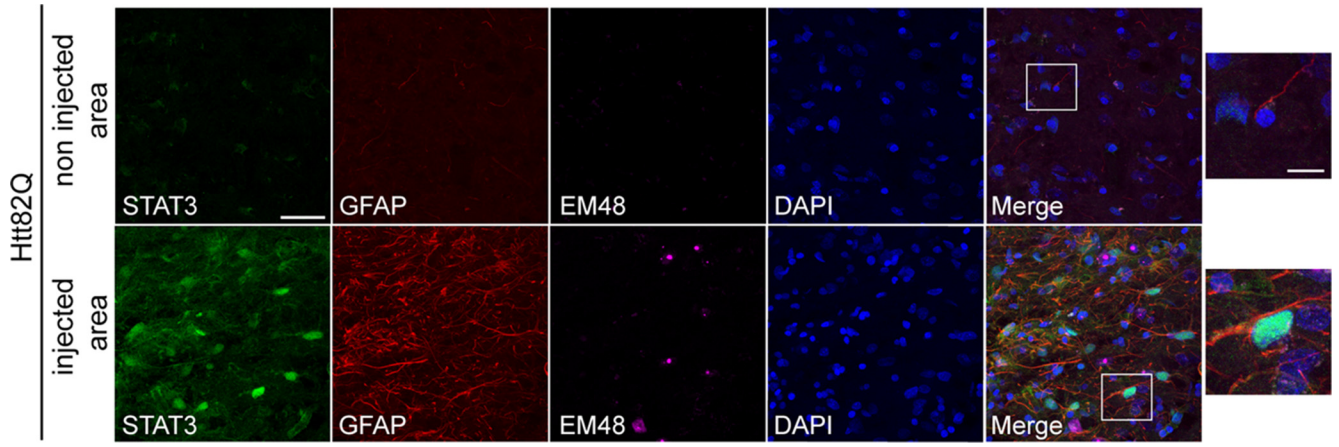

Figure 5. The JAK/STAT3 pathway is activated in reactive astrocytes in the primate model of HD. ***A***, Images of brain sections from macaques injected with lenti-Htt82Q in the putamen showing triple staining for STAT3 (green), GFAP (red), and EM48 (magenta). Seventeen months after infection with lenti-Htt82Q in the putamen, EM48$^+$ aggregates of mHtt are observed, as well as prominent astrocyte reactivity. The immunoreactivity for STAT3 is much stronger in GFAP$^+$ reactive astrocytes than in resting astrocytes found outside the injected area in the same animal. Images are representative of all three macaques. Scale bars: 40 μm; enlargement, 10 μm.

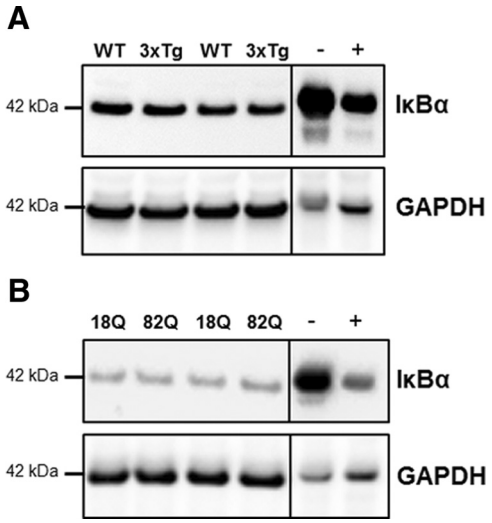

Figure 6. The NF-κB pathway is not activated in 3xTg-AD mice and the lentiviral-based model of HD. Western blot for IκBα and GAPDH in 3xTg-AD mice (3xTg) or their age-matched WT controls (***A***) or mice injected in the left striatum with lenti-Htt18Q (18Q) and in the right striatum with lenti-Htt82Q (82Q; ***B***). IκBα expression is similar between 3xTg-AD and WT mice and between the left and right striatum of mice injected with lenti-Htt. The abundance of IκBα is lower in HeLa cells treated with TNFα (positive control, +) than in untreated cells (negative control, −). $n = 4–6$ mice per group.

We injected lenti-SOCS3 plus lenti-GFP or lenti-GFP alone into the subiculum of 7- to 8-month-old 3xTg-AD mice, and we analyzed the mice 4.5 months later. The subiculum was chosen because it is the region displaying the most prominent accumulation of amyloid plaques and astrocyte reactivity at this age (Oddo et al., 2003; Fig. 1*C*). In 3xTg-AD mice, SOCS3 strongly decreased STAT3 expression in astrocytes (Fig. 7*A*). The number of GFP$^+$ astrocytes showing STAT3 immunoreactivity in the nucleus was significantly lower in mice coinfected with lenti-SOCS3 than in those infected with lenti-GFP alone ($p = 0.0375$, df = 6, Student's *t* test; Fig. 7*B*). SOCS3 overexpression visibly reduced GFAP expression in the subiculum (Fig. 7*C*). GFAP expression was 73% lower in the SOCS3 group than in the GFP controls, although this difference was not statistically significant ($p = 0.0827$, df = 6, Student's *t* test; Fig. 7*D*). There were significantly fewer GFP$^+$ astrocytes coexpressing GFAP in the SOCS3 group than in the control (−94%, $p = 0.0149$, df = 6, Student's *t* test; Fig. 7*E*). GFP expression in infected astrocytes allowed us to visualize their morphology in both groups. Astrocytes in the subiculum of 3xTg-AD mice displayed a morphology characteristic of reactive astrocytes with enlarged soma and large GFAP$^+$ primary processes (Fig. 7*A*,*C*,*F*). In contrast, SOCS3-infected astrocytes displayed complex ramifications composed of thin cytoplasmic processes organized radially around the soma (Fig. 7*A*,*C*,*F*), typical of resting astrocytes of the mouse brain (Wilhelmsson et al., 2006). We also performed immunostaining for S100β, a ubiquitous marker of astrocytes, to verify that SOCS3 did not globally impair protein expression in astrocytes. The number of GFP$^+$/S100β^+ astrocytes was similar between 3xTg-AD mice injected with lenti-SOCS3 or lenti-GFP (Fig. 7*F*,*G*).

We performed the same experiment with the lentiviral-based model of HD. C57BL/6 mice were injected with lenti-Htt82Q and lenti-GFP in the left striatum and with lenti-Htt82Q, lenti-SOCS3, and lenti-GFP in the right striatum at the same total virus load. Again, SOCS3 efficiently prevented the activation of the JAK/STAT3 pathway in astrocytes (Fig. 8*A*). The number of infected cells coexpressing STAT3 was 87% lower in the striatum injected with lenti-SOCS3 than in the control striatum ($p = 0.0072$, df = 3, Student's paired *t* test; Fig. 8*B*). In addition, the percentage of cells highly fluorescent for STAT3 was strongly reduced by SOCS3 ($p = 0.0118$, df = 3, Student's paired *t* test; Fig. 8*C*). SOCS3-expressing astrocytes displayed a bushy morphology with thin cytoplasmic processes and numerous ramifications, whereas reactive astrocytes in the control striatum showed enlarged and tortuous primary processes (Fig. 8*A*,*D*,*G*). Inhibition of the JAK/STAT3 pathway by SOCS3 prevented the increase of GFAP expression in the lenti-Htt82Q-injected area (Fig. 8*D*). The GFAP$^+$ area was 86% smaller in the striatum injected with lenti-SOCS3 than in the control striatum ($p = 0.0035$, df = 3, Student's paired *t* test; Fig. 8*E*). In addition, the number of GFP$^+$/GFAP$^+$ cells was significantly decreased by SOCS3 ($p = 0.0036$, df = 3, Student's paired *t* test, Fig. 8*F*). On the contrary, the number of GFP$^+$/S100β^+ astrocytes was not altered by SOCS3 (Fig. 8*G*,*H*).

Activation of the JAK/STAT3 pathway results in the transcriptional activation of many genes, including *gfap* and *vimentin*. Therefore, we studied the mRNA abundance of reactive astrocyte markers to characterize further the effect of SOCS3 expression in astrocytes. We only used the lentiviral-based HD model, because

the infected area in the subiculum of 3xTg-AD mice was too small to be dissected out for qRT-PCR analysis. We studied the effects of lenti-SOCS3 on mice injected with lenti-Htt18Q or lenti-Htt82Q compared with the control vector lenti-GFP by performing a two-way (Htt length and treatment) ANOVA. *gfap* mRNA was induced more than twofold by lenti-Htt82Q (Fig. 8*J*), consistent with immunofluorescence results. Expression of SOCS3 in astrocytes normalized the expression of *gfap* to levels comparable with controls ($p = 0.0254$ for Htt length × treatment effect, df = 1, two-way ANOVA; Fig. 8*J*). A similar pattern was observed with *vimentin* mRNA ($p = 0.0018$ for Htt length × treatment effect, df = 1, two-way ANOVA; Fig. 8*K*). Importantly, SOCS3 overexpression in mice injected with the control lentiviral vector lenti-Htt18Q did not change *gfap* or *vimentin* expression, showing that SOCS3 has no effect in resting astrocytes. These results suggest that inhibition of the JAK/STAT3 pathway in reactive astrocytes restores a resting-like status to astrocytes.

Preventing astrocyte reactivity reduces neuroinflammation

We then evaluated how the inhibition of astrocyte reactivity affected other pathological features (neuroinflammation, protein aggregation, and neuronal death).

We first studied the expression of IBA1, a marker of microglia that is upregulated during microglial activation attributable to both transcriptional regulation and morphological changes (Sieber et al., 2013). The IBA1$^+$ area was 38% smaller in the striatum injected with lenti-SOCS3 than in the control striatum ($p = 0.0397$, df = 5, Student's paired *t* test; Fig. 9*A*,*B*). A similar effect was observed in the subiculum of 3xTg-AD mice injected with lenti-SOCS3, although it did not reach significance (−44%, $p = 0.1800$, df = 5, Student's *t* test; data not shown). We also studied the neuroinflammatory response at the transcriptional level. The expression of the microglial marker *aif1* (*iba1*) was increased 2.3-fold by Htt82Q and reduced by SOCS3 ($p = 0.0048$ for Htt length × treatment effect, df = 1, two-way ANOVA; Fig. 9*C*). Similarly, the marker for reactive microglia *itgam* (CD11b) and the chemokine *ccl2* were increased 2.3- and 4.1-fold, respectively, by Htt82Q and reduced to control levels by SOCS3 ($p = 0.0165$ and $p < 0.0001$, respectively, for Htt length × treatment effect, df = 1, two-way ANOVA; Fig.

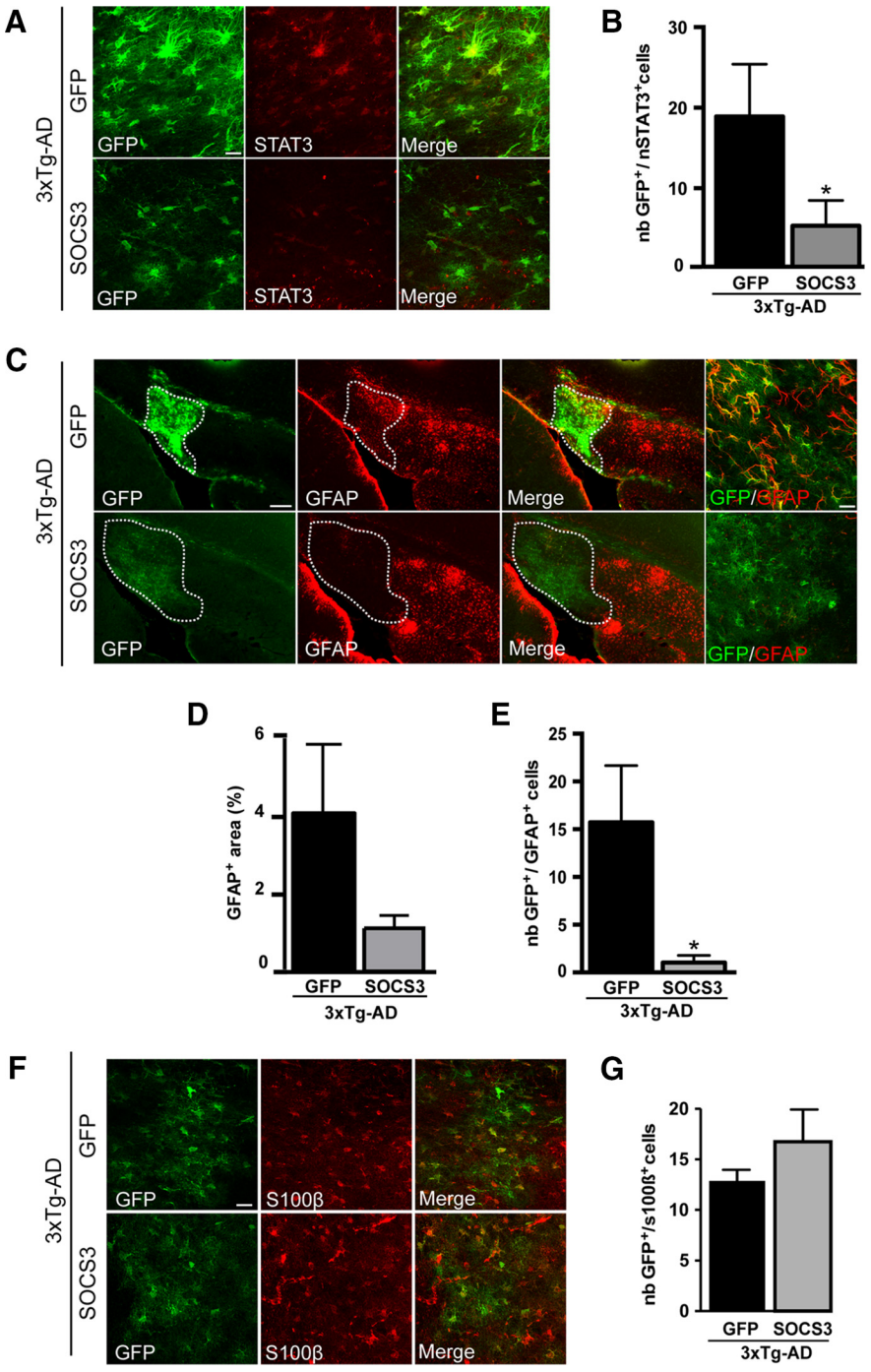

Figure 7. The JAK/STAT3 pathway is responsible for astrocyte reactivity in 3xTg-AD mice. ***A***, Images of double staining for GFP (green) and STAT3 (red) in 7- to 8-month-old 3xTg-AD mice injected in the subiculum with lenti-GFP or lenti-SOCS3 plus lenti-GFP (same total virus load). STAT3 expression becomes undetectable in astrocytes infected with lenti-SOCS3. ***B***, The number of GFP$^+$ astrocytes coexpressing STAT3 in the nucleus (GFP$^+$/nSTAT3$^+$ cells) is significantly lower in the SOCS3 group than in the GFP control group. ***C***, Images of GFP (green) and GFAP (red) staining in brain sections from 3xTg-AD mice injected with lenti-GFP or lenti-SOCS3 plus lenti-GFP in the subiculum. Lenti-SOCS3 injection strongly reduces GFAP expression in the injected area (delimited by white dots) in 3xTg-AD mice. Note that infected astrocytes in the SOCS3 group have a bushy morphology typical of resting astrocytes, whereas cells in the GFP group are hypertrophic with enlarged primary processes. ***D***, Quantification of the GFAP$^+$ area in 3xTg-AD mice injected with lenti-SOCS3 plus lenti-GFP or lenti-GFP alone. ***E***, The number of GFP$^+$ astrocytes coexpressing GFAP is significantly lower in the SOCS3 group than in the GFP control group. ***F***, Immunofluorescent labeling for the astrocyte marker S100β. ***G***, Quantification of the number of infected astrocytes coexpressing S100β (GFP$^+$/S100β^+ cells) shows that its expression is not altered by SOCS3. $n = 3$–5 per group. *$p < 0.05$. Scale bars: ***A*** and ***F***, 20 μm; ***C***, left, 500 μm; right, 20 μm. Infected astrocytes in both groups are identified by their expression of GFP.

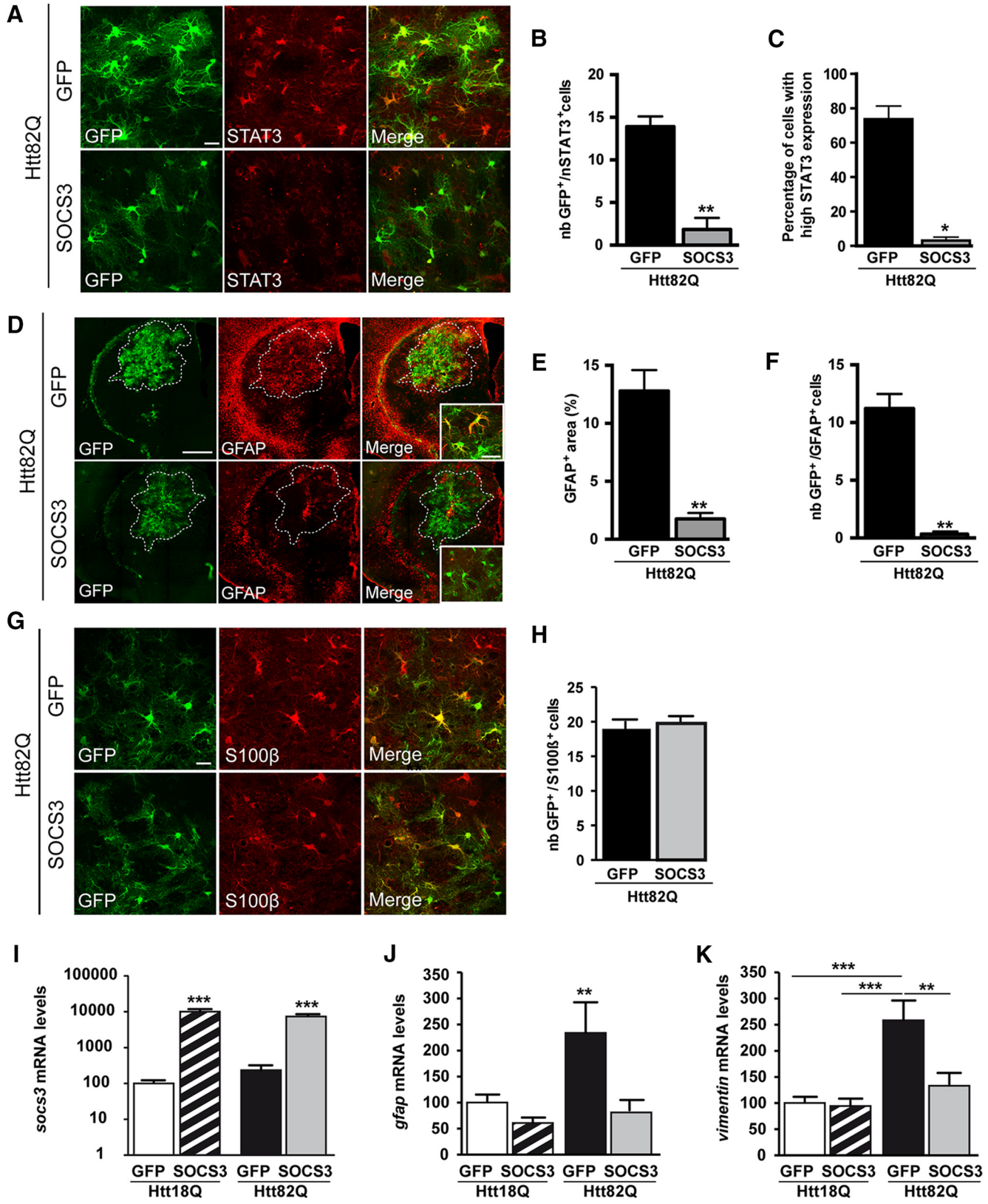

Figure 8. The JAK/STAT3 pathway is responsible for astrocyte reactivity in the lentiviral-based mouse model of HD. ***A***, Immunofluorescent staining of GFP (green) and STAT3 (red) in mice injected in the left striatum with lenti-Htt82Q plus lenti-GFP and the right striatum with lenti-Htt82Q plus lenti-SOCS3 plus lenti-GFP. STAT3 expression becomes undetectable in astrocytes infected with lenti-SOCS3. ***B***, ***C***, The number of GFP $^{+}$/nSTAT3 $^{+}$ astrocytes (***B***) and the percentage of cells showing strong staining for STAT3 (***C***) is significantly lower in the right striatum injected with lenti-SOCS3 than in the control striatum. ***D***, SOCS3 expression strongly reduces GFAP expression (red) in the injected area (GFP $^{+}$, green). Infected astrocytes in the SOCS3 group display thin processes and complex ramifications, unlike hypertrophic reactive astrocytes in the control group. ***E***, Quantification confirms that the GFAP $^{+}$ area is significantly smaller in the striatum injected with lenti-SOCS3 than in the control striatum. ***F***, The number of GFP $^{+}$ astrocytes coexpressing GFAP is significantly lower in the striatum expressing SOCS3 than in the control striatum. ***G***, Immunofluorescent staining for the astrocyte marker S100β (red). ***H***, The number of GFP $^{+}$/S100β $^{+}$ cells is not different between the two groups. ***I–K***, qRT-PCR analysis on mice injected in the striatum (*Figure legend continues.*)

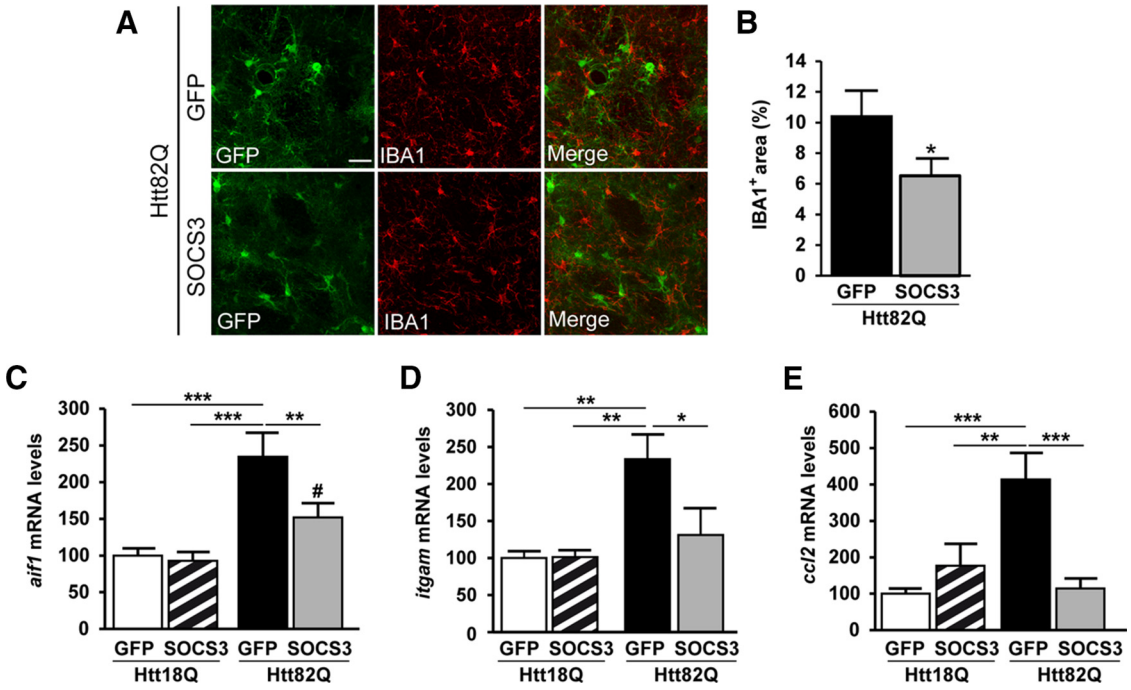

Figure 9. Preventing astrocyte reactivity reduces microglial activation. ***A***, Immunofluorescent staining of GFP (green) and IBA1 (red) in mice injected in the left striatum with lenti-Htt82Q plus lenti-GFP and the right striatum with lenti-Htt82Q plus lenti-SOCS3 plus lenti-GFP. ***B***, Quantification shows that the IBA1$^+$ area is significantly smaller in the striatum injected with lenti-SOCS3 than in the control striatum. ***C–E***, qRT-PCR analysis on mice injected in the striatum with lenti-Htt18Q plus lenti-GFP, lenti-Htt18Q plus lenti-SOCS3 plus lenti-GFP, lenti-Htt82Q plus lenti-GFP, or lenti-Htt82Q plus lenti-SOCS3 plus lenti-GFP (same total virus load). The expression of *aif1* (*iba1*; ***C***), *itgam* (*CD11b*; ***D***), and *ccl2* (***E***) is induced by lenti-Htt82Q and is reduced by SOCS3. $n = 4–11$ per group. $^*p < 0.05$, $^{**}p < 0.01$, $^{***}p < 0.001$, $^{\#}p < 0.05$ versus Htt18Q plus GFP and Htt18Q plus SOCS3. Scale bar, 20 μm.

9*D*,*E*). These results suggest that inhibition of astrocyte reactivity reduces the neuroinflammatory response.

Preventing astrocyte reactivity modulates HD pathology

Finally, we evaluated the effects of SOCS3 on neuronal death and mHtt aggregation. Htt82Q induced a lesion detected by a loss of DARPP32 staining and COX activity. SOCS3 did not change the size of the lesion as measured with these two markers ($p = 0.2088$ and $p = 0.1508$, respectively, df = 10, Student's paired *t* test; Fig. 10). However, SOCS3 significantly increased the number of EM48$^+$ mHtt aggregates ($p = 0.0409$, df = 10, Student's paired *t* test; Fig. 10). The average size of EM48$^+$ aggregates was not different between the GFP and SOCS3 groups (GFP, 10.20 ± 0.30 μm^2; SOCS3, 10.60 ± 0.48 μm^2, $p = 0.3638$).

Overall, our results identify the JAK/STAT3 pathway as a pivotal and universal signaling cascade for astrocyte reactivity in various models of ND. Inhibition of the JAK/STAT3 pathway in reactive astrocytes influences several disease outcomes in the context of HD.

Discussion

Activation of the JAK/STAT3 pathway is a universal feature of astrocyte reactivity

The JAK/STAT3 pathway is known to trigger astrocyte reactivity in models of acute injury (Kang and Hébert, 2011). We aimed to decipher the role of the JAK/STAT3 pathway in astrocyte reactivity during progressive pathological conditions, such as ND.

Active pSTAT3 could not be detected by immunohistochemistry; therefore, we used increased STAT3 expression and nuclear localization as alternative indicators of pathway activation, as described previously by us and others (Escartin et al., 2006; Tyzack et al., 2014). The absence of pSTAT3 immunoreactivity was not attributable to a technical problem because we were able to detect it with the positive control CNTF. Instead, it may be attributable to the models of ND themselves, which are progressive and may involve low, transient, or asynchronous phosphorylation of STAT3. We show that the JAK/STAT3 pathway is activated in reactive astrocytes in mouse models of both AD and HD and in a primate model of HD.

Importantly, the etiology of the two ND studied here is very different and involves particular vulnerable brain regions. Thus, activation of the JAK/STAT3 pathway appears to be a universal feature of astrocyte reactivity, observed in multiple brain disorders, both acute and progressive. Both resting and reactive astrocytes are now considered as highly heterogeneous cells in terms of their morphological or functional features (Anderson et al., 2014). However, our results suggest that the molecular cascades triggering reactivity are in fact highly conserved between disease states, species, and brain regions.

In addition to the three mouse models studied here, we examined astrocyte reactivity in two transgenic mouse models of HD. Both N171-82Q and Hdh140 mice display behavioral abnormalities and striatal atrophy. However, we did not observe substantial astrocyte reactivity in end-stage N171-82Q mice or before 17 months of age in Hdh140 mice. Interestingly, the JAK/STAT3 pathway was also found activated in the few reactive astrocytes of the old Hdh140 mouse. This limited astrocyte reactivity in HD transgenic mice is consistent with the literature (Tong et al.,

←

(*Figure legend continued.*) with lenti-Htt18Q plus lenti-GFP, lenti-Htt18Q plus lenti-SOCS3 plus lenti-GFP, lenti-Htt82Q plus lenti-GFP, or lenti-Htt82Q plus lenti-SOCS3 plus lenti-GFP (same total virus load). ***I***, *Socs3* mRNA is overexpressed >100 times after lenti-SOCS3 injection. The expression of *gfap* (***J***) and *vimentin* (***K***) is induced by lenti-Htt82Q and is restored to levels observed in the Htt18Q controls by the expression of SOCS3. Note that lenti-SOCS3 has no effect in resting astrocytes. $n = 4–11$ per group. $^*p < 0.05$, $^{**}p < 0.01$, $^{***}p < 0.001$. Scale bars: ***A*** and ***G***, 20 μm; ***D***, 500 μM; enlargement, 20 μm.

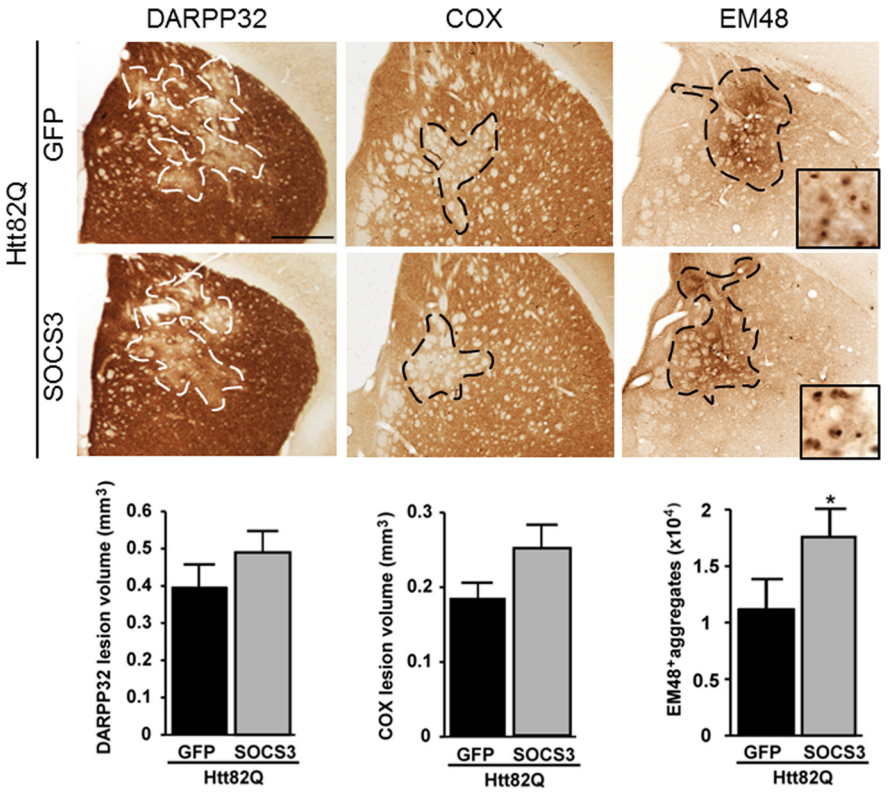

Figure 10. Preventing astrocyte reactivity modulates HD pathology. Immunostaining of the striatal neuronal marker DARPP32 and histochemistry of COX in mice injected in the left striatum with lenti-Htt82Q plus lenti-GFP and in the right striatum with lenti-Htt82Q plus lenti-SOCS3 plus lenti-GFP. mHtt aggregates are detected by immunostaining with EM48 in the same mice, and they form nuclear inclusions (see enlargement). Quantification of the lesion size and the number of EM48$^+$ aggregates. SOCS3 increases the number of EM48$^+$ aggregates. $n = 11$. $^*p < 0.05$. Scale bar, 500 μm.

2014) but differs greatly from what is observed in HD patients (Faideau et al., 2010). This discrepancy may be related to the absence of massive neuronal death in HD transgenic models. Thus, we focused on the lentiviral-based model of HD that reproduces neuronal death in the striatum, along with strong astrocyte reactivity.

Astrocyte reactivity in ND models is mediated by the JAK/STAT3 pathway

By immunohistological and biochemical techniques, it was shown that the JAK/STAT3 pathway is activated in reactive astrocytes in several models of acute injury (Justicia et al., 2000; Xia et al., 2002) and in ALS (Shibata et al., 2010). Experiments involving pharmacological inhibitors of the JAK/STAT3 pathway later suggested that this pathway was needed for astrocyte reactivity, including in the MPTP model of PD (Sriram et al., 2004). However, the JAK/STAT3 pathway is active in all brain cells; therefore, it is possible that such inhibitors affect other cell types besides astrocytes. More recently, genetic approaches have been developed to knock out the expression of STAT3 specifically in astrocytes with the Cre–LoxP system. STAT3 conditional knock-out strongly reduces astrocyte reactivity after acute injuries (Okada et al., 2006; Herrmann et al., 2008; Tyzack et al., 2014). However, the use of a non-inducible Cre recombinase expressed under a *nestin* or *gfap* promoter may trigger side effects, because these promoters are active during embryonic development (Alvarez-Buylla et al., 2001). In contrast, our strategy based on SOCS3 overexpression by lentiviral gene transfer results in an efficient inhibition of the JAK/STAT3 pathway specifically in astrocytes of the adult brain. Indeed, SOCS3 was able to prevent the accumulation of STAT3 in the nucleus of reactive astrocytes in ND models and to blunt the strong phosphorylation of STAT3 induced by CNTF. This selective approach allowed us to demonstrate that the JAK/STAT3 pathway is responsible for astrocyte reactivity in two models of ND.

In agreement with a pivotal role of the JAK/STAT3 pathway for astrocyte reactivity, we observed no evidence for an activation of the NF-κB pathway in these models. This pathway is associated with astrocyte reactivity in acute disorders, such as spinal cord injury (Kang and Hébert, 2011). In AD and HD, the NF-κB pathway is altered in neurons (Chiba et al., 2009; Khoshnan and Patterson, 2011) but is activated in the peripheral immune cells of HD patients (Träger et al., 2014) and in astrocytes in mouse models of both diseases (Hsiao et al., 2013; Medeiros and LaFerla, 2013). However, the specific requirement of this pathway for the establishment of reactivity in astrocytes has not been tested in these NDs. The NF-κB pathway is activated mainly in microglial cells in the SOD^{G93A} mouse model of ALS (Frakes et al., 2014). Indeed, inhibition of the NF-κB pathway in astrocytes reduced their reactivity very moderately and only transiently (Crosio et al., 2011). In both studies, inhibition of the NF-κB pathway in astrocytes did not influence disease outcomes, further suggesting that this pathway does not play a major role in reactive astrocytes during ND.

There are multiple levels of crosstalk between the NF-κB and the JAK/STAT3 pathways (Fan et al., 2013). It is possible that the NF-κB pathway secondarily activates the JAK/STAT3 pathway or that STAT3 inhibits the NF-κB pathway (Yu et al., 2002). Although other signaling pathways may be active in astrocytes or in other cell types during the disease, our experiments based on the specific inhibition by SOCS3 in astrocytes show that the JAK/STAT3 pathway is ultimately responsible for triggering astrocyte reactivity in these ND.

Viral vectors are versatile tools; therefore, our approach based on a lentiviral vector encoding an inhibitor of the JAK/STAT3 pathway could be easily extended to any animal model of brain disease, including those affecting different brain regions. However, one limitation is that lentiviral vectors may transduce a small number of cells, especially in the subiculum, preventing qRT-PCR or biochemical analysis by Western blotting.

What are the effects of STAT3-mediated astrocyte reactivity?

The JAK/STAT3 pathway is a ubiquitous signaling pathway involved in cell proliferation, survival, and differentiation (Levy and Darnell, 2002). In adult astrocytes, activation of the JAK/STAT3 pathway increases the expression of cytoskeletal proteins, such as GFAP and vimentin, as observed here, but many other genes could be induced, as shown in reactive astrocytes after ischemia or LPS injection *in vivo* (Zamanian et al., 2012). In particular, reactive astrocytes may release several signaling molecules,

such as cytokines or chemokines, that affect neighboring cells, including microglial cells (Burda and Sofroniew, 2014). Indeed, we found an increased expression of neuroinflammation markers in the lenti-based model of HD, which was restored to basal levels by SOCS3. This observation suggests that reactive astrocytes are responsible for microglial activation in this model and illustrates the complex dialog occurring between glial cells in ND.

Blunting astrocyte reactivity by SOCS3 also increased the number of mHtt aggregates, suggesting that reactive astrocytes participate in mHtt processing and aggregation. Because those mHtt aggregates are found mainly in neurons, such an effect necessarily involves neuron-to-astrocyte communication. Interestingly, it was reported recently that mHtt can propagate between neurons (Pecho-Vrieseling et al., 2014), opening the possibility that it may also be exchanged between neurons and glial cells. More experiments are needed to decipher the molecular mechanisms responsible for the control of mHtt clearance by reactive astrocytes.

It is still highly debated how mHtt inclusions contribute to neuronal death: it may be toxic, protective, or without effect (Arrasate and Finkbeiner, 2012). We show that increasing the number of mHtt aggregates does not influence the lesion, which is in favor of a disconnection between mHtt aggregates and neuronal death. Indeed, the inclusions of mHtt measured here are only the end products of mHtt metabolism, and it is now believed that soluble or oligomeric mHtt are the toxic species (Leitman et al., 2013).

We show that interfering with astrocyte reactivity influences two important features of HD (neuroinflammation and mHtt aggregation) but did not affect neuronal death. However, we cannot exclude that the lentiviral-based model of HD is too severe to allow restoration by the modulation of astrocyte and microglia reactivity or mHtt aggregation.

A similar thorough evaluation of SOCS3 effects could not be performed in the 3xTg-AD model because the volume targeted with lenti-SOCS3 was too small to provide a reliable quantification of disease indexes, such as amyloid load. There are conflicting reports on the role of reactive astrocytes in AD (Furman et al., 2012; Kraft et al., 2013). It may be clarified by inhibiting the JAK/STAT3 pathway, identified here as an instrumental cascade to promote reactivity, and assessing the consequences on AD outcomes.

Our study extends previous findings obtained in acute models of injury and suggests that the JAK/STAT3 pathway is a universal signaling cascade involved in virtually all pathological situations in the brain. Manipulation of the JAK/STAT3 pathway is a promising strategy to study the functional features of reactive astrocyte, as well as their contribution to disease progression, particularly in the context of ND.

References

Alvarez-Buylla A, García-Verdugo JM, Tramontin AD (2001) A unified hypothesis on the lineage of neural stem cells. Nat Rev Neurosci 2:287–293. CrossRef Medline

Anderson MA, Ao Y, Sofroniew MV (2014) Heterogeneity of reactive astrocytes. Neurosci Lett 565:23–29. CrossRef Medline

Arrasate M, Finkbeiner S (2012) Protein aggregates in Huntington's disease. Exp Neurol 238:1–11. CrossRef Medline

Bjørbaek C, Elmquist JK, Frantz JD, Shoelson SE, Flier JS (1998) Identification of SOCS-3 as a potential mediator of central leptin resistance. Mol Cell 1:619–625. CrossRef Medline

Bonni A, Frank DA, Schindler C, Greenberg ME (1993) Characterization of a pathway for ciliary neurotrophic factor signaling to the nucleus. Science 262:1575–1579. CrossRef Medline

Burda JE, Sofroniew MV (2014) Reactive gliosis and the multicellular response to CNS damage and disease. Neuron 81:229–248. CrossRef Medline

Campbell IL, Erta M, Lim SL, Frausto R, May U, Rose-John S, Scheller J, Hidalgo J (2014) Trans-signaling is a dominant mechanism for the pathogenic actions of interleukin-6 in the brain. J Neurosci 34:2503–2513. CrossRef Medline

Chiba T, Yamada M, Sasabe J, Terashita K, Shimoda M, Matsuoka M, Aiso S (2009) Amyloid-beta causes memory impairment by disturbing the JAK2/STAT3 axis in hippocampal neurons. Mol Psychiatry 14:206–222. CrossRef Medline

Colin A, Faideau M, Dufour N, Auregan G, Hassig R, Andrieu T, Brouillet E, Hantraye P, Bonvento G, Déglon N (2009) Engineered lentiviral vector targeting astrocytes in vivo. Glia 57:667–679. CrossRef Medline

Crosio C, Valle C, Casciati A, Iaccarino C, Carrì MT (2011) Astroglial inhibition of NF-kappaB does not ameliorate disease onset and progression in a mouse model for amyotrophic lateral sclerosis (ALS). PLoS One 6:e17187. CrossRef Medline

Damiano M, Diguet E, Malgorn C, D'Aurelio M, Galvan L, Petit F, Benhaim L, Guillermier M, Houitte D, Dufour N, Hantraye P, Canals JM, Alberch J, Delzescaux T, Déglon N, Beal MF, Brouillet E (2013) A role of mitochondrial complex II defects in genetic models of Huntington's disease expressing N-terminal fragments of mutant huntingtin. Hum Mol Genet 22:3869–3882. CrossRef Medline

de Almeida LP, Ross CA, Zala D, Aebischer P, Déglon N (2002) Lentiviral-mediated delivery of mutant huntingtin in the striatum of rats induces a selective neuropathology modulated by polyglutamine repeat size, huntingtin expression levels, and protein length. J Neurosci 22:3473–3483. Medline

Escartin C, Bonvento G (2008) Targeted activation of astrocytes: a potential neuroprotective strategy. Mol Neurobiol 38:231–241. CrossRef Medline

Escartin C, Brouillet E, Gubellini P, Trioulier Y, Jacquard C, Smadja C, Knott GW, Kerkerian-Le Goff L, Déglon N, Hantraye P, Bonvento G (2006) Ciliary neurotrophic factor activates astrocytes, redistributes their glutamate transporters GLAST and GLT-1 to raft microdomains, and improves glutamate handling in vivo. J Neurosci 26:5978–5989. CrossRef Medline

Faideau M, Kim J, Cormier K, Gilmore R, Welch M, Auregan G, Dufour N, Guillermier M, Brouillet E, Hantraye P, Déglon N, Ferrante RJ, Bonvento G (2010) In vivo expression of polyglutamine-expanded huntingtin by mouse striatal astrocytes impairs glutamate transport: a correlation with Huntington's disease subjects. Hum Mol Genet 19:3053–3067. CrossRef Medline

Fan Y, Mao R, Yang J (2013) NF-kappaB and STAT3 signaling pathways collaboratively link inflammation to cancer. Protein Cell 4:176–185. CrossRef Medline

Frakes AE, Ferraiuolo L, Haidet-Phillips AM, Schmelzer L, Braun L, Miranda CJ, Ladner KJ, Bevan AK, Foust KD, Godbout JP, Popovich PG, Guttridge DC, Kaspar BK (2014) Microglia induce motor neuron death via the classical NF-kappaB pathway in amyotrophic lateral sclerosis. Neuron 81:1009–1023. CrossRef Medline

Francelle L, Galvan L, Gaillard MC, Guillermier M, Houitte D, Bonvento G, Petit F, Jan C, Dufour N, Hantraye P, Elalouf JM, de Chaldee M, Deglon N, Brouillet E (2014) Loss of the thyroid hormone binding protein Crym renders striatal neurons more vulnerable to mutant huntingtin in Huntington's disease. Hum Mol Genet. Advance online publication. Retrieved January 8, 2015. doi:10.1093/hmg/ddu571. CrossRef Medline

Furman JL, Sama DM, Gant JC, Beckett TL, Murphy MP, Bachstetter AD, Van Eldik LJ, Norris CM (2012) Targeting astrocytes ameliorates neurologic changes in a mouse model of Alzheimer's disease. J Neurosci 32:16129–16140. CrossRef Medline

Hamby ME, Sofroniew MV (2010) Reactive astrocytes as therapeutic targets for CNS disorders. Neurotherapeutics 7:494–506. CrossRef Medline

Hayden MS, Ghosh S (2008) Shared principles in NF-kappaB signaling. Cell 132:344–362. CrossRef Medline

Herrmann JE, Imura T, Song B, Qi J, Ao Y, Nguyen TK, Korsak RA, Takeda K, Akira S, Sofroniew MV (2008) STAT3 is a critical regulator of astrogliosis and scar formation after spinal cord injury. J Neurosci 28:7231–7243. CrossRef Medline

Hottinger AF, Azzouz M, Déglon N, Aebischer P, Zurn AD (2000) Complete and long-term rescue of lesioned adult motoneurons by lentiviral-mediated expression of glial cell line-derived neurotrophic factor in the facial nucleus. J Neurosci 20:5587–5593. Medline

Hsiao HY, Chen YC, Chen HM, Tu PH, Chern Y (2013) A critical role of astrocyte-mediated nuclear factor-kappaB-dependent inflammation in Huntington's disease. Hum Mol Genet 22:1826–1842. CrossRef Medline

Itagaki S, McGeer PL, Akiyama H, Zhu S, Selkoe D (1989) Relationship of microglia and astrocytes to amyloid deposits of Alzheimer disease. J Neuroimmunol 24:173–182. CrossRef Medline

Jankowsky JL, Fadale DJ, Anderson J, Xu GM, Gonzales V, Jenkins NA, Copeland NG, Lee MK, Younkin LH, Wagner SL, Younkin SG, Borchelt DR (2004) Mutant presenilins specifically elevate the levels of the 42 residue beta-amyloid peptide in vivo: evidence for augmentation of a 42-specific gamma secretase. Hum Mol Genet 13:159–170. CrossRef Medline

Justicia C, Gabriel C, Planas AM (2000) Activation of the JAK/STAT pathway following transient focal cerebral ischemia: signaling through Jak1 and Stat3 in astrocytes. Glia 30:253–270. CrossRef Medline

Kang W, Hébert JM (2011) Signaling pathways in reactive astrocytes, a genetic perspective. Mol Neurobiol 43:147–154. CrossRef Medline

Kershaw NJ, Murphy JM, Liau NP, Varghese LN, Laktyushin A, Whitlock EL, Lucet IS, Nicola NA, Babon JJ (2013) SOCS3 binds specific receptor-JAK complexes to control cytokine signaling by direct kinase inhibition. Nat Struct Mol Biol 20:469–476. CrossRef Medline

Khoshnan A, Patterson PH (2011) The role of IkappaB kinase complex in the neurobiology of Huntington's disease. Neurobiol Dis 43:305–311. CrossRef Medline

Kraft AW, Hu X, Yoon H, Yan P, Xiao Q, Wang Y, Gil SC, Brown J, Wilhelmsson U, Restivo JL, Cirrito JR, Holtzman DM, Kim J, Pekny M, Lee JM (2013) Attenuating astrocyte activation accelerates plaque pathogenesis in APP/PS1 mice. FASEB J 27:187–198. CrossRef Medline

Leitman J, Ulrich Hartl F, Lederkremer GZ (2013) Soluble forms of polyQ-expanded huntingtin rather than large aggregates cause endoplasmic reticulum stress. Nat Commun 4:2753. CrossRef Medline

Levy DE, Darnell JE Jr (2002) Stats: transcriptional control and biological impact. Nat Rev Mol Cell Biol 3:651–662. CrossRef Medline

Medeiros R, LaFerla FM (2013) Astrocytes: conductors of the Alzheimer disease neuroinflammatory symphony. Exp Neurol 239:133–138. CrossRef Medline

Menalled LB, Sison JD, Dragatsis I, Zeitlin S, Chesselet MF (2003) Time course of early motor and neuropathological anomalies in a knock-in mouse model of Huntington's disease with 140 CAG repeats. J Comp Neurol 465:11–26. CrossRef Medline

Naldini L, Blömer U, Gallay P, Ory D, Mulligan R, Gage FH, Verma IM, Trono D (1996) In vivo gene delivery and stable transduction of nondividing cells by a lentiviral vector. Science 272:263–267. CrossRef Medline

O'Callaghan JP, Kelly KA, VanGilder RL, Sofroniew MV, Miller DB (2014) Early activation of STAT3 regulates reactive astrogliosis induced by diverse forms of neurotoxicity. PLoS One 9:e102003. CrossRef Medline

Oddo S, Caccamo A, Shepherd JD, Murphy MP, Golde TE, Kayed R, Metherate R, Mattson MP, Akbari Y, LaFerla FM (2003) Triple-transgenic model of Alzheimer's disease with plaques and tangles: intracellular Abeta and synaptic dysfunction. Neuron 39:409–421. CrossRef Medline

Okada S, Nakamura M, Katoh H, Miyao T, Shimazaki T, Ishii K, Yamane J, Yoshimura A, Iwamoto Y, Toyama Y, Okano H (2006) Conditional ablation of Stat3 or Socs3 discloses a dual role for reactive astrocytes after spinal cord injury. Nat Med 12:829–834. CrossRef Medline

Palfi S, Brouillet E, Jarraya B, Bloch J, Jan C, Shin M, Condé F, Li XJ, Aebischer P, Hantraye P, Déglon N (2007) Expression of mutated huntingtin fragment in the putamen is sufficient to produce abnormal movement in non-human primates. Mol Ther 15:1444–1451. CrossRef Medline

Pecho-Vrieseling E, Rieker C, Fuchs S, Bleckmann D, Esposito MS, Botta P, Goldstein C, Bernhard M, Galimberti I, Müller M, Lüthi A, Arber S, Bouwmeester T, van der Putten H, Di Giorgio FP (2014) Transneuronal propagation of mutant huntingtin contributes to non-cell autonomous pathology in neurons. Nat Neurosci 17:1064–1072. CrossRef Medline

Probst A, Ulrich J, Heitz PU (1982) Senile dementia of Alzheimer type: astroglial reaction to extracellular neurofibrillary tangles in the hippocampus. An immunocytochemical and electron-microscopic study. Acta Neuropathol 57:75–79. CrossRef Medline

Ruan L, Kang Z, Pei G, Le Y (2009) Amyloid deposition and inflammation in APPswe/PS1dE9 mouse model of Alzheimer's disease. Curr Alzheimer Res 6:531–540. CrossRef Medline

Ruiz M, Déglon N (2012) Viral-mediated overexpression of mutant huntingtin to model HD in various species. Neurobiol Dis 48:202–211. CrossRef Medline

Schilling G, Becher MW, Sharp AH, Jinnah HA, Duan K, Kotzuk JA, Slunt HH, Ratovitski T, Cooper JK, Jenkins NA, Copeland NG, Price DL, Ross CA, Borchelt DR (1999) Intranuclear inclusions and neuritic aggregates in transgenic mice expressing a mutant N-terminal fragment of huntingtin. Hum Mol Genet 8:397–407. CrossRef Medline

Shibata N, Kakita A, Takahashi H, Ihara Y, Nobukuni K, Fujimura H, Sakoda S, Sasaki S, Iwata M, Morikawa S, Hirano A, Kobayashi M (2009) Activation of signal transducer and activator of transcription-3 in the spinal cord of sporadic amyotrophic lateral sclerosis patients. Neurodegener Dis 6:118–126. CrossRef Medline

Shibata N, Yamamoto T, Hiroi A, Omi Y, Kato Y, Kobayashi M (2010) Activation of STAT3 and inhibitory effects of pioglitazone on STAT3 activity in a mouse model of SOD1-mutated amyotrophic lateral sclerosis. Neuropathology 30:353–360. CrossRef Medline

Sieber MW, Jaenisch N, Brehm M, Guenther M, Linnartz-Gerlach B, Neumann H, Witte OW, Frahm C (2013) Attenuated inflammatory response in triggering receptor expressed on myeloid cells 2 (TREM2) knock-out mice following stroke. PLoS One 8:e52982. CrossRef Medline

Sofroniew MV, Vinters HV (2010) Astrocytes: biology and pathology. Acta Neuropathol 119:7–35. CrossRef Medline

Sriram K, Benkovic SA, Hebert MA, Miller DB, O'Callaghan JP (2004) Induction of gp130-related cytokines and activation of JAK2/STAT3 pathway in astrocytes precedes up-regulation of glial fibrillary acidic protein in the 1-methyl-4-phenyl-1,2,3,6-tetrahydropyridine model of neurodegeneration: key signaling pathway for astrogliosis in vivo? J Biol Chem 279:19936–19947. CrossRef Medline

Starr R, Willson TA, Viney EM, Murray LJ, Rayner JR, Jenkins BJ, Gonda TJ, Alexander WS, Metcalf D, Nicola NA, Hilton DJ (1997) A family of cytokine-inducible inhibitors of signalling. Nature 387:917–921. CrossRef Medline

Tong X, Ao Y, Faas GC, Nwaobi SE, Xu J, Haustein MD, Anderson MA, Mody I, Olsen ML, Sofroniew MV, Khakh BS (2014) Astrocyte Kir4.1 ion channel deficits contribute to neuronal dysfunction in Huntington's disease model mice. Nat Neurosci 17:694–703. CrossRef Medline

Träger U, Andre R, Lahiri N, Magnusson-Lind A, Weiss A, Grueninger S, McKinnon C, Sirinathsinghji E, Kahlon S, Pfister EL, Moser R, Hummerich H, Antoniou M, Bates GP, Luthi-Carter R, Lowdell MW, Björkqvist M, Ostroff GR, Aronin N, Tabrizi SJ (2014) HTT-lowering reverses Huntington's disease immune dysfunction caused by NFkappaB pathway dysregulation. Brain 137:819–833. CrossRef Medline

Tyzack GE, Sitnikov S, Barson D, Adams-Carr KL, Lau NK, Kwok JC, Zhao C, Franklin RJ, Karadottir RT, Fawcett JW, Lakatos A (2014) Astrocyte response to motor neuron injury promotes structural synaptic plasticity via STAT3-regulated TSP-1 expression. Nat Commun 5:4294. CrossRef Medline

Vonsattel JP, Myers RH, Stevens TJ, Ferrante RJ, Bird ED, Richardson EP Jr (1985) Neuropathological classification of Huntington's disease. J Neuropathol Exp Neurol 44:559–577. CrossRef Medline

Wilhelmsson U, Bushong EA, Price DL, Smarr BL, Phung V, Terada M, Ellisman MH, Pekny M (2006) Redefining the concept of reactive astrocytes as cells that remain within their unique domains upon reaction to injury. Proc Natl Acad Sci U S A 103:17513–17518. CrossRef Medline

Xia XG, Hofmann HD, Deller T, Kirsch M (2002) Induction of STAT3 signaling in activated astrocytes and sprouting septal neurons following entorhinal cortex lesion in adult rats. Mol Cell Neurosci 21:379–392. CrossRef Medline

Yu ZX, Li SH, Evans J, Pillarisetti A, Li H, Li XJ (2003) Mutant huntingtin causes context-dependent neurodegeneration in mice with Huntington's disease. J Neurosci 23:2193–2202. Medline

Yu Z, Zhang W, Kone BC (2002) Signal transducers and activators of transcription 3 (STAT3) inhibits transcription of the inducible nitric oxide synthase gene by interacting with nuclear factor kappaB. Biochem J 367:97–105. CrossRef Medline

Zamanian JL, Xu L, Foo LC, Nouri N, Zhou L, Giffard RG, Barres BA (2012) Genomic analysis of reactive astrogliosis. J Neurosci 32:6391–6410. CrossRef Medline